Current Optics and Photonics
Vol. 4, No. 6, December 2020, pp. 558-565

ISSN: 2508-7266(Print) / ISSN: 2508-7274(Online)
DOI: https://doi.org/10.3807/COPP.2020.4.6.558

Proposal for a Wavelength-Independent Optical Sensor Based on an Asymmetric Mach-Zehnder Interferometer

Yanxia Luo, Rui Yin*, Wei Ji, Qingjie Huang, Zisu Gong, and Jingyao Li**

Department of Electronic Science and Technology, School of Information Science and Engineering, Shandong University, Qingdao 266237, China

(Received September 16, 2020 : revised November 13, 2020 : accepted November 17, 2020)

A wavelength-independent optical sensor based on an asymmetric Mach-Zehnder interferometer (AMZI) is proposed. The optical sensor based on an AMZI is very sensitive to wavelength, and wavelength drift will lead to measurement error. The optical sensor is compensated to reduce its dependence on wavelength. The insensitivity of the optical sensor to wavelength mainly depends on the compensation structure, which is composed of an AMZI cascaded with another AMZI and can compensate the wavelength drift. The influence of wavelength drift on the optical sensor can be counteracted by carefully designing the size parameters of the compensation structure. When the wavelength changes from 1549.9 nm to 1550.1 nm, the error after compensation can be lower than 0.066%. Furthermore, the effect of fabrication tolerance on compensation results is analyzed. The proposed compensation method can also be used to compensate the drift of other parameters such as temperature, and can be applied to the compensation of other interference-based optical devices.

Keywords : Optical pressure sensor, Wavelength independent, Asymmetric Mach-Zehnder interferometer, Compensation structure
OCIS codes : (220.4610) Optical fabrication; (230.7380) Waveguides, channeled; (280.4788) Optical sensing and sensors

I. INTRODUCTION

A complex optical system requires many kinds of optical devices, such as a laser, optical fiber, optical switching device, optical delay device, nonlinear optical device, optical modulator, detector, optical attenuator, optical gyroscope, optical sensor. Moreover, many optical devices adopt the principle of interference, such as those based on the AMZI [1-3] or Fabry-Perot (FP) cavity [4, 5], which feature low insertion loss, simple structure, and ease of manufacture, and are widely used in the fields of optical-fiber communication and sensing. These include AMZI-based optical filters [6], optical amplifiers [7], optical switches, AMZI-coupled ring resonators [8], and optical sensors [9-13]; optical devices based on the FP cavity include lasers [14], erbium-doped fiber lasers, tunable filters [15], various optical sensors [16-19], and more. Most of the sensors based on the AMZI or FP cavity perceive the change in measurement parameters by detecting intensity, but nonmeasurement parameters can have an impact on the sensor's measurement results. For an optical sensor based on an AMZI, changes in wavelength also affect the measurement results. The relationship between the nonmeasurement parameters and output light intensity of the sensor satisfies a sinusoidal curve. In addition, the relationship between wavelength and output light intensity of an interference optical device is also sinusoidal. Therefore, the influence of many non-measurement parameters on output light intensity of an interference optical device is similar to that of wavelength on the output light intensity of an AMZI.

*Corresponding author: yinrui@sdu.edu.cn, ORCID 0000-0003-3959-040X
**Corresponding author: Jiwww@sdu.edu.cn, ORCID 0000-0001-8460-9312

Color versions of one or more of the figures in this paper are available online.

The wavelength drift of the light source is derived from the aging of the light source itself, and the change in the ambient temperature. In this study the influence of the light source's wavelength drift on the system is analyzed. According to the actual application scenario, the wavelength range of the light source is set to determine the influence of wavelength change on the system. The transfer function of the output of the optical sensor with a change in wavelength is analyzed. Then, through the compensation structure we design, it is used to compensate the wavelength drift of the optical sensor based on an AMZI. Furthermore, better compensation can be obtained by optimizing the size of the structure. The proposed optical compensation structure is composed of an AMZI optical sensor cascaded with another AMZI. The error before and after compensation is analyzed. The results show that a well-designed compensation structure can reduce the influence of wavelength on the optical sensor. This compensation mechanism also can be used to compensate the drift of other nonmeasurement parameters, and can be applied to other interference-based optical devices.

II. BASIC THEORY

For an AMZI structure, the relationship between wavelength and output light intensity is sinusoidal, and many other optical devices have a similar transmission curve, such as the FP cavity and the directional coupler (DC).

For a DC with waveguide width of 0.5 μm, waveguide spacing of 0.1 μm, core and cladding refractive indices of 3.4 and 1.0 respectively, and couple length of 1 mm, the transmission curve is represented by red the dashed line in Fig. 1. The result for a FP cavity with cavity width of 48.4365 μm and refractive index of 1.46 is represented by the green dash-dotted line in Fig. 1. An AMZI with arm-length difference of 96.873 μm and waveguide effective refractive index of 1.46 is also indicated in Fig. 1, by the blue solid line.

Figure 1 shows that the three curves basically coincide. Therefore, the transmission curves of many optical devices whose working principle is interference can be equivalent to that of an AMZI.

A general AMZI structure is shown in Fig. 2. It consists of two couplers and two interference arms of different lengths. After the light wave enters, it is divided along two paths by the 3-dB coupler. After passing through the two interference arms of lengths L_1 and L_2, and another 3-dB coupler, the light waves traveling along the two paths interfere and combine into a single output light wave. When sensing, under the influence of changes in the external environment the optical waveguide will expand or contract and the refractive index will change, which will cause the optical-path difference and phase between the two arms to change. The optical-path difference changes as

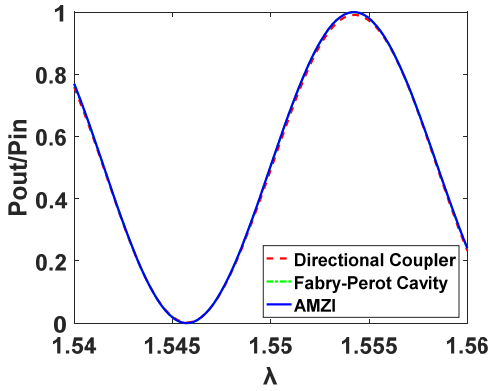

FIG. 1. Output light intensity versus wavelength, for a DC, FP cavity, and AMZI.

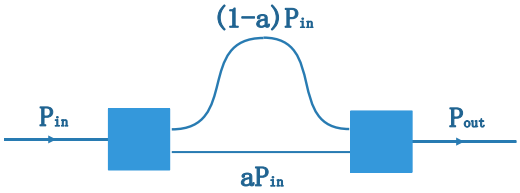

FIG. 2. Structural diagram of an AMZI.

$$\Delta L = L_1 - L_2 . \tag{1}$$

The phase difference between the two arms changes as

$$\Delta\varphi = \frac{2\pi}{\lambda}\cdot n_{eff}\cdot \Delta L . \tag{2}$$

The ratio of output power to input power can be expressed as

$$P_{out}/P_{in} = \frac{1}{2}(1+\cos\Delta\varphi) . \tag{3}$$

In these expressions P_{out} is the output power, P_{in} is the input power, Δφ is the phase difference between the two interference arms of the AMZI, λ is the wavelength, n_{eff} is the effective refractive index of the waveguide, and ΔL is the length difference between the two interference arms of the AMZI.

For a general AMZI structure, the power ratio between L_1 and L_2 is a:(1-a). In waveguide optics this can be realized by a multimode interference structure [20]. The output light's power can be expressed as

$$\begin{aligned} P_{out} &= \left[aE_{in}e^{i\Delta\varphi} + (1-a)E_{in}\right]\cdot\left[aE_{in}e^{i\Delta\varphi} + (1-a)E_{in}\right]^* \\ &= [aE_{in}(\cos\Delta\varphi + i\sin\Delta\varphi) + (1-a)E_{in}]\cdot[aE_{in}(\cos\Delta\varphi + i\sin\Delta\varphi) + (1-a)E_{in}]^* \\ &= [(a\cos\Delta\varphi + 1 - a) + ia\sin\Delta\varphi]E_{in}\cdot[(a\cos\Delta\varphi + 1 - a) - ia\sin\Delta\varphi]E_{in} \\ &= P_{in}[(a\cos\Delta\varphi + 1 - a)^2 - (ia\sin\Delta\varphi)^2] \\ &= P_{in}\left[2a^2 - 2a + 1 + (2a - 2a^2)\cos\Delta\varphi\right], \end{aligned} \tag{4}$$

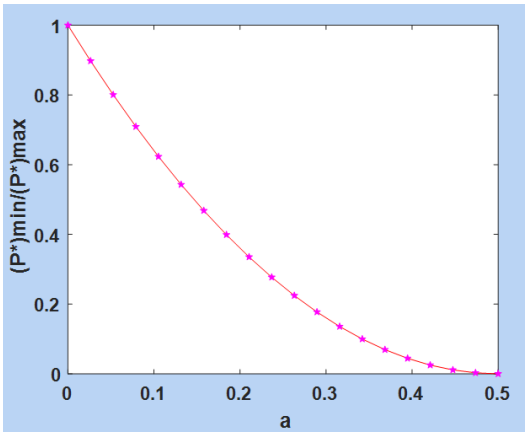

FIG. 3. $(P^*)_{\min} / (P^*)_{\max}$ of an AMZI for different values of a.

where E_{in} is the electric field intensity of the input light, and P_{in} and P_{out} are the input and output optical power respectively. Letting $b = 2a^2 - 2a + 1$, we can obtain

$$\frac{P_{out}}{P_{in}} = b + (1-b)\cos\Delta\varphi \,. \tag{5}$$

We next define $P^* = P_{out} / P_{in}$. The $(P^*)_{\min} / (P^*)_{\max}$ of the AMZI changes with a, as shown by the pink curve in Fig. 3. When a changes from 0 to 0.5 and from 0.5 to 1, the corresponding $(P^*)_{\min} / (P^*)_{\max}$ curve is symmetric with respect to $a = 0.5$.

III. COMPENSATION PRINCIPLE

The output of the optical sensor is very sensitive to the wavelength, and wavelength drift causes great sensing error. To make the optical sensor function normally in a working environment, it is necessary to eliminate the influence of other parameters. Using the inherent characteristic of the AMZI, that is, the output changes with wavelength, the error caused by wavelength drift can be compensated. It is found that adding an AMZI structure in front of or behind the original AMZI structure has an obvious effect on compensation for wavelength drift.

The optical sensor based on an AMZI is compensated, and the schematic diagram of a self-compensating optical sensor is shown in Fig. 4. It consists of two AMZIs in series: one is the sensing AMZI, and the other is the compensating AMZI. The refractive index of the compensation area does not change with the external environment, while the refractive index of the sensing area does. The AMZI's power splitter and coupler are in asymmetric multimode interference, which can realize any proportion of power distribution [20]. Through a compensating structure, the influence of wavelength drift on the sensor can be curtailed, and the stability and accuracy of the sensor can be improved.

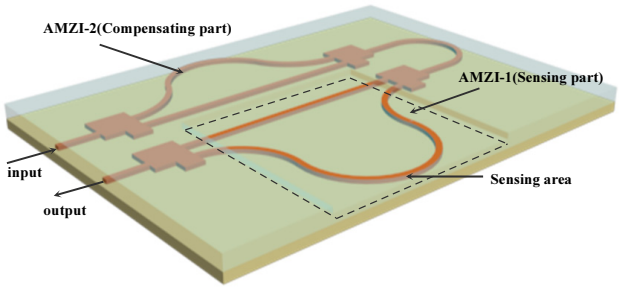

FIG. 4. Schematic diagram of the optical compensation structure.

According to Eq. (5), the transmission function of the sensing AMZI can be expressed as

$$\left(\frac{P_{out}}{P_{in}}\right)_1 = b_1 + (1-b_1)\cos\Delta\varphi_1 \,, \tag{6}$$

where $\Delta\varphi_1 = 2\pi \cdot n_{eff1} \cdot \Delta L_1/\lambda$ is the phase difference between the two arms of the sensing AMZI, and n_{eff1} and ΔL_1 are the effective refractive index and arm-length difference of the sensing AMZI respectively.

The compensating AMZI's transmission function can be expressed as

$$\left(\frac{P_{out}}{P_{in}}\right)_2 = b_2 + (1-b_2)\cos\Delta\varphi_2 \,, \tag{7}$$

where $\Delta\varphi_2 = 2\pi \cdot n_{eff2} \cdot \Delta L_2/\lambda$ is the phase difference between the two arms of the compensating AMZI, and n_{eff2} and ΔL_2 are the effective refractive index and arm-length difference of the compensating AMZI respectively.

Adjusting the arm-length difference can change the phase difference between the two AMZIs. The phases of the AMZIs are

$$\Delta\varphi_1 = \frac{2\pi}{\lambda_0} \cdot n_s(x) \cdot \Delta L_1 \,, \quad \Delta\varphi_2 = \frac{2\pi}{\lambda_0} \cdot n_1 \cdot \Delta L_2 \,, \tag{8}$$

where $n_s(x)$ is the refractive index that changes with the sensing environment, and x is the sensing parameter (temperature, pressure, etc.). In the initial state x_0, we have $n_s(x) = n_1$. By this point, thus

$$\Delta\varphi_2 = \Delta\varphi_1 + \Phi \,, \tag{9}$$

$$\Phi = \frac{2\pi}{\lambda_0} \cdot n_1 \cdot \Delta L_2 - \frac{2\pi}{\lambda_0} \cdot n_1 \cdot \Delta L_1 = \frac{2\pi}{\lambda_0} \cdot n_1 \cdot dL \,, \tag{10}$$

where Φ (value 0-2π) is the difference in phase differences between the two AMZIs, and dL is the difference in arm-length differences between the AMZIs.

The final sensing curve can be expressed as

$$\left(\frac{P_{out}}{P_{in}}\right)_{final}=\left(\frac{P_{out}}{P_{in}}\right)_1\times\left(\frac{P_{out}}{P_{in}}\right)_2 =\left[b_1+(1-b_1)\cos\Delta\varphi_1\right]\cdot\left[b_2+(1-b_2)\cos\Delta\varphi_2\right]. \tag{11}$$

When $x=x_0$, the final sensing curve can be expressed as

$$\left(\frac{P_{out}}{P_{in}}\right)_{final}=\left(\frac{P_{out}}{P_{in}}\right)_1\times\left(\frac{P_{out}}{P_{in}}\right)_2 =\left[b_1+(1-b_1)\cos\frac{2\pi}{\lambda_0}\cdot n_1\cdot\Delta L_1\right] \cdot\left[b_2+(1-b_2)\cos(\frac{2\pi}{\lambda_0}\cdot n_1\cdot\Delta L_2+\Phi)\right]. \tag{12}$$

When the wavelength does not drift, the final sensing curve can be written as

$$\left(\frac{P_{out}}{P_{in}}\right)_{final}=\left(\frac{P_{out}}{P_{in}}\right)_1\times\left(\frac{P_{out}}{P_{in}}\right)_2 =\left[b_1+(1-b_1)\cos\frac{2\pi}{\lambda_0}\cdot n_s(x)\cdot\Delta L_1\right] \cdot\left[b_2+(1-b_2)\cos(\frac{2\pi}{\lambda_0}\cdot n_1\cdot\Delta L_2+\Phi)\right]. \tag{13}$$

When the wavelength drifts negatively to $\lambda_1(\lambda_1-\Delta\lambda)$, the final sensing curve can be written as

$$\left(\frac{P_{out}}{P_{in}}\right)_{final}'=\left(\frac{P_{out}}{P_{in}}\right)_1'\times\left(\frac{P_{out}}{P_{in}}\right)_2' =\left[b_1+(1-b_1)\cos\frac{2\pi}{\lambda_1}\cdot n_s(x)\cdot\Delta L_1\right] \cdot\left[b_2+(1-b_2)\cos(\frac{2\pi}{\lambda_1}\cdot n_1\cdot\Delta L_2+\frac{\lambda_1}{\lambda_0}\cdot\Phi)\right]. \tag{14}$$

When the wavelength drifts positively to $\lambda_2(\lambda_1+\Delta\lambda)$, the final sensing curve can be written as

$$\left(\frac{P_{out}}{P_{in}}\right)_{final}''=\left(\frac{P_{out}}{P_{in}}\right)_1''\times\left(\frac{P_{out}}{P_{in}}\right)_2'' =\left[b_1+(1-b_1)\cos\frac{2\pi}{\lambda_2}\cdot n_s(x)\cdot\Delta L_1\right] \cdot\left[b_2+(1-b_2)\cos(\frac{2\pi}{\lambda_2}\cdot n_1\cdot\Delta L_2+\frac{\lambda_2}{\lambda_0}\cdot\Phi)\right]. \tag{15}$$

If t_1 represents the transmission curve of the central wavelength λ_0, t_2 represents the transmission curve of the central wavelength negatively drifted to λ_1, and t_3 represents the transmission curve of the central wavelength positively drifted to λ_2. The maximum sensing error E_{max} after wavelength drift is expressed as

$$E_{\max}=\max\{\frac{\max[t_1(\lambda),t_2(\lambda),t_3(\lambda)]-\min[(t_1(\lambda),t_2(\lambda),t_3(\lambda)]}{t_1(\lambda)}\},\lambda\in[\lambda_1,\lambda_2]. \tag{16}$$

$[\lambda_1,\lambda_2]$ is the range of wavelength drift, and E_{max} is the maximum sensing error within the sensing range of refractive-index change, $[n_1,n_2]$.

IV. DESIGN OPTIMIZATION AND PERFORMANCE ANALYSIS OF COMPENSATION STRUCTURE

E_{max} can be reduced by adjusting b_1, b_2, ΔL_1, and ΔL_2. In the following analysis the wavelength-drift range is 1549.9-1550.1 nm. We take a SiO_2 sensor as the first example for compensation.

First, the influence of Φ on sensing is analyzed as follows: Set the effective refractive-index range of the sensor to be [1.46,1.4601]. Therefore the effective refractive index of the compensating AMZI is 1.46. The values of b_1 and b_2 are both 0.8, and ΔL_1 is 425.386116915 μm. Φ changes with ΔL_2. Figure 5 shows the trend of E_{max} with Φ; it can be seen that the sensing error is smaller when $\Phi=1.2\pi$.

Next, the influence of b_1 and b_2 on the sensor is analyzed.

According to the results of Fig. 5, let $\Phi=1.2\pi$ and $\Delta L_1=425.386116915$ μm. Figure 6 shows the trend of E_{max} changing with b_1 and b_2, and it can be seen that a smaller E_{max} can be realized when $b_1=b_2$. Figure 7 shows the value of E_{max} when $b_1=b_2$; it can be seen that when $b_1=b_2=0.8$, E_{max} is about 0.1034, reaching the minimum.

Finally, when $\Phi=1.2\pi$ and $b_1=b_2=0.8$, there are multiple options for ΔL_1 and ΔL_2. The value of AMZI arm-length difference ΔL_1 is analyzed, and the results are shown

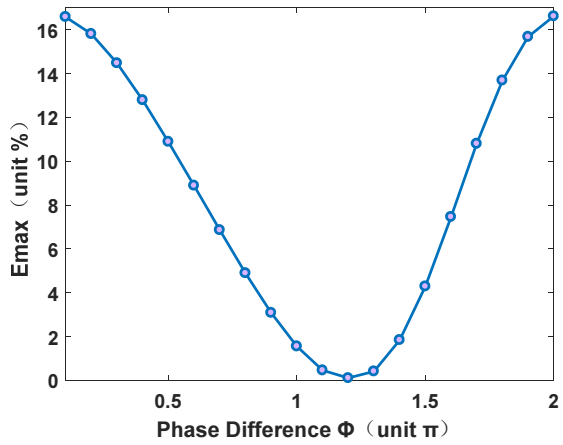

FIG. 5. Different Φ values corresponding to E_{max}.

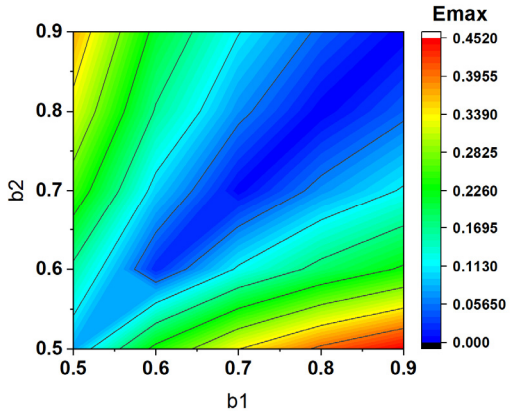

FIG. 6. Contour map of E_{max} varying with b_1 and b_2.

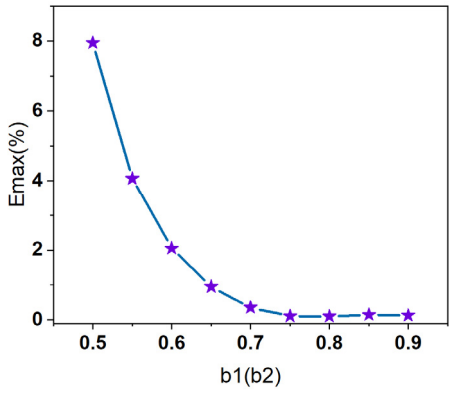

FIG. 7. E_{max} corresponding to different b values.

in Table 1. This table shows that E_{max} increases with increasing of ΔL_1. In other words, for a specified value of E_{max}, the smaller the arm length difference, the larger the effective-index dynamic range of the sensor. The maximum sensing error and the dynamic range of effective-index change can be measured according to the demands of the specific application.

TABLE 1. E_{max} corresponding to different arm-length differences ΔL_1 of the sensing AMZI

Sensing AMZI arm length difference ΔL_1 (μm)	E_{max} (%)	Sensing AMZI arm length difference ΔL_1 (μm)	E_{max} (%)
106.903873155	0.006155	510.314715251	0.1527
213.064621075	0.024750	605.859388379	0.2226
319.225368995	0.056670	701.404061507	0.3097
425.386116915	0.103400	807.564809427	0.4295

TABLE 2. Parameter design of optical sensors, and comparison before and after compensation

Waveguide material	ΔL_1 (μm)	ΔL_2 (μm)	Before compensation	After compensation
			E_{max} (%)	E_{max} (%)
SiO_2	425.386116915	426.0083	8.351	0.06606
$LiNbO_3$	310.486125316	310.8981	9.176	0.05493
Si	200.904398465	201.1701	9.174	0.03569

After another round of optimization, when $b_1 = b_2 = 0.8$, $\Delta L_1 = 425.386116915$ μm, and $\Delta L_2 = 426.00832669$ μm ($\Phi = 1.175\pi$), E_{max} is reduced to 0.06606%.

The compensation of optical sensors based on lithium niobate and silicon is also analyzed in the same way. The refractive index of lithium niobate is about 2.2, and that of silicon is about 3.4. The sensing area of the lithium niobate sensor is set to be [2.2,2.2001], and that of the silicon sensor is set as [3.4,3.4001]. The b value of the AMZI is 0.8. The parameter design and results before and after compensation of the optical sensors are shown in Table 2. It can be seen that for the three materials, the sensing error

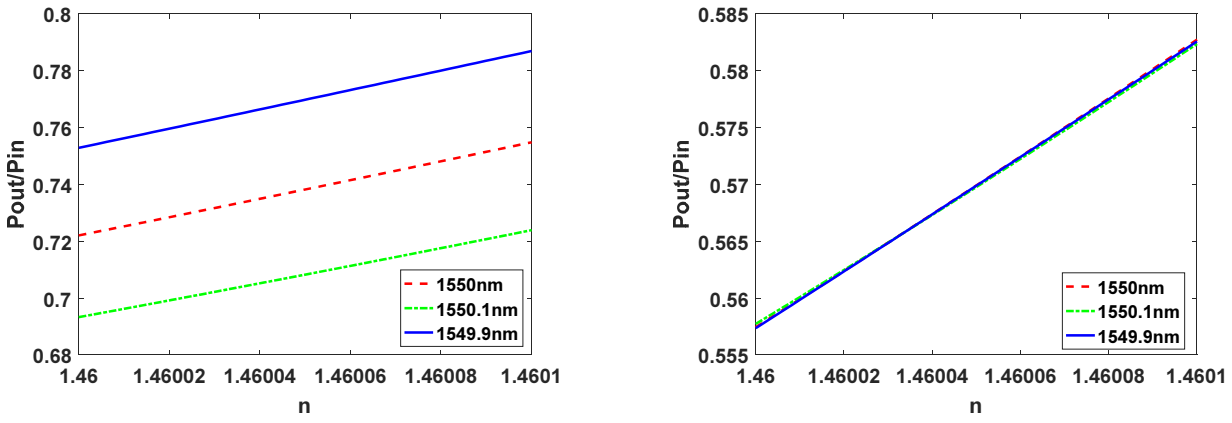

(a) (b)

FIG. 8. Comparison of sensing curves between (a) uncompensated and (b) compensated systems, based on a silicon dioxide optical sensor.

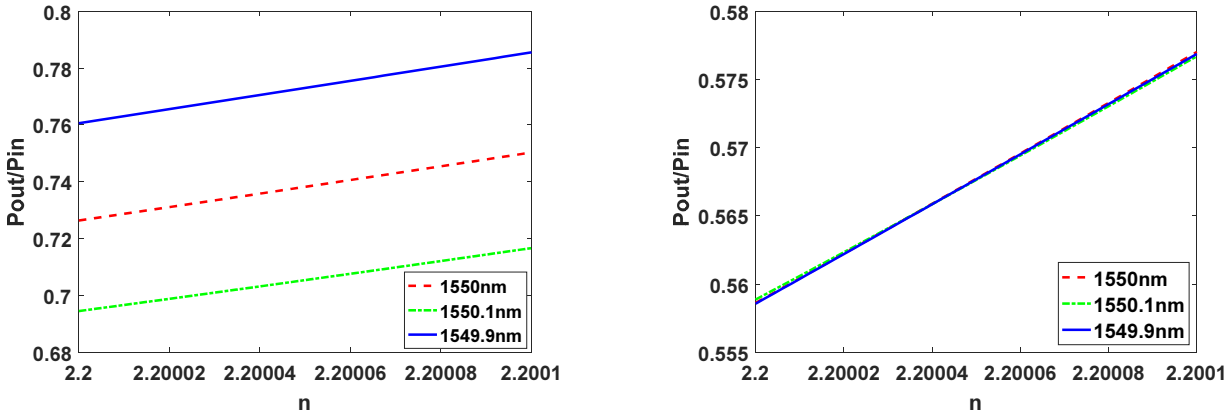

FIG. 9. For the optical sensor made of lithium niobate, the comparison of the sensing curves between (a) uncompensated and (b) compensated systems.

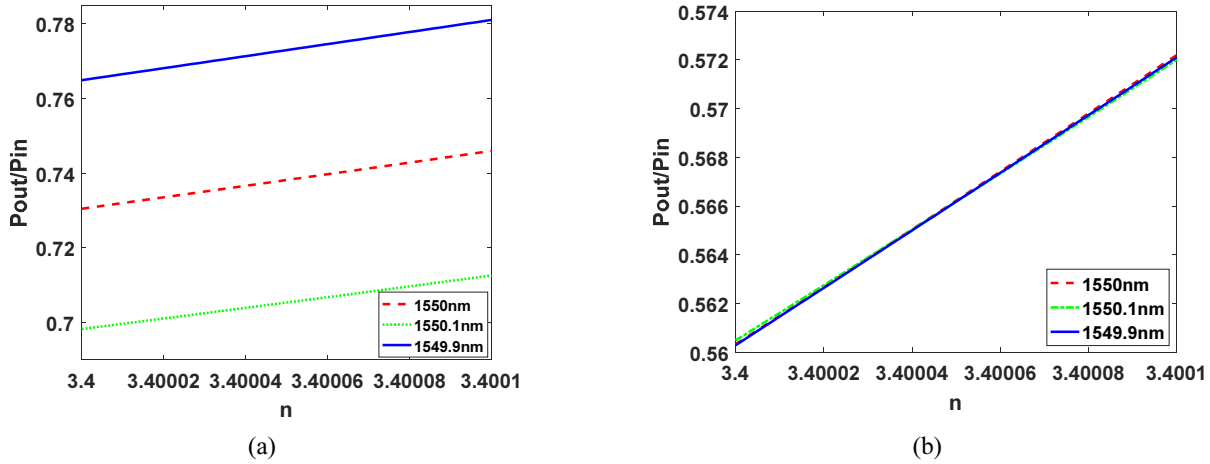

FIG. 10. Based on the silicon optical sensor, the comparison of the sensing curves between (a) uncompensated and (b) compensated systems.

is reduced from 8-9% to below 0.066% in some cases.

The sensing curves before and after compensation in Table 2 are shown in Figs. 8, 9, and 10 respectively. It can be seen that the compensated results are satisfying, and the sensing curves almost coincide.

V. FABRICATION TOLERANCE ANALYSIS

In this section, the influence of the error in the sensor-fabrication process is analyzed using a two-dimensional calculation.

The influence of waveguide width on the measurement results is analyzed. The width of the waveguide layer is 4 μm, the refractive index of the core layer is 1.464821, and that of the cladding layer is 1.45. When the width of the waveguide increases or decreases by 0.1 μm, the Transverse Electric (TE) effective index of the waveguide changes to 1.4601374 and 1.459857, respectively. For this situation, the sensing curve after compensation is shown in Fig. 11. The maximum error in Fig. 11(a) is 0.2406%, and that in Fig. 11(b) is 0.7284%.

Generally, the influence of the fabrication process on the length of the two interference arms of the AMZI is the same, so ΔL is almost constant. In spite of this, the change in sensing curve when ΔL has errors due to other special reasons is analyzed. Figure 12 shows the sensing curve when the arm-length difference of the two AMZIs increases or decreases by 0.1μm at the same time. The maximum error in Fig. 12(a) is 0.3713%, and that in Fig. 12(b) is 1.007%.

From Figs. 11 and 12, the error caused by the manufacturing process is not conducive to sensing. A change in waveguide width will change the effective-index range and increase the sensing error, and error in arm-length difference will also increase sensing error. Nonetheless, for a manufacturing error of ±0.1 μm, the measurement error can still be held below 1%.

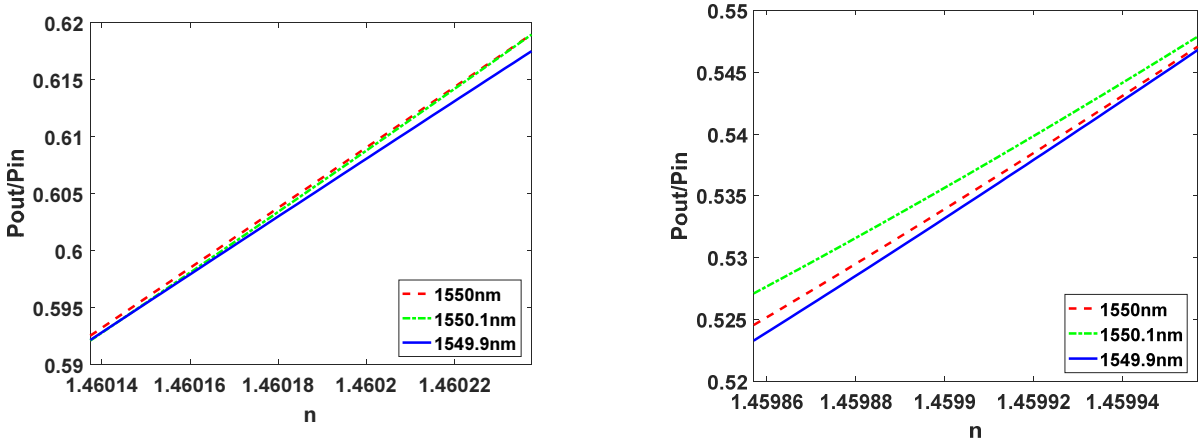

(a) (b)

FIG. 11. Sensing curves when the waveguide's width (a) increases or (b) decreases by 0.1 μm.

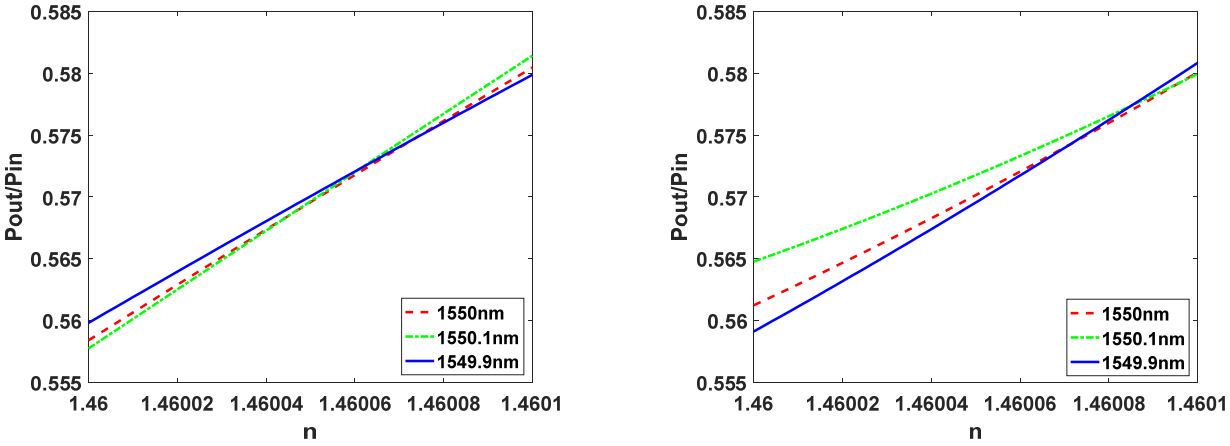

(a) (b)

FIG. 12. The sensing curve when the arm-length difference of the two AMZIs (a) increases or (b) decreases by 0.1 μm.

VI. CONCLUSION

A wavelength-independent optical sensor based on the AMZI is introduced. The compensation structure consists of two AMZIs in series, one as a sensor and the other as a compensator. For optical sensors based on silicon dioxide, lithium niobate, and silicon, the transmission curves with and without a compensation structure are analyzed. The error when using a compensation structure is less than 0.066%, which is only 0.8% of without compensation. At the same time, the variation range of output light intensity after compensation is reduced to about 78% of that without compensation. Finally, the fabrication tolerance is analyzed, and the sensing error can be less than 1% for a fabrication tolerance of ±0.1 μm. This compensation structure could also be used to compensate for the drift of other nonmeasurement parameters, such as temperature, and could be applied to other interference-based optical devices.

ACKNOWLEDGMENT

This study is supported by the National Natural Science Foundation of China (Grant 61571273, Grant 61771292, and Grant 31430031-2), the Key Technology Research and Development Program of Shandong (2017YFC0803403, 2018YFC0831103), and the Fundamental Research Funds of Hisense Broadband.

REFERENCES

1. C. G. Martinez and R. R. Trejo, "Remotely biasing the electro-optic response of an electric field sensing-detection system using $LiNbO_3$ asymmetric Mach-Zehnder optical retarders," Appl. Opt. **57**, 9677-9682 (2018).
2. M. Ren, X. Li, J. Zhang, L. Wang, Y. Wang, H. Wang, J. Li, X. Yin, Y. Wu, and J. An, "Optimization of the classical interference visibility of an asymmetric Mach-

Zehnder interferometer based on planar lightwave circuit technology," Appl. Opt. **58**, 7817-7822 (2019).
3. L. Liu, L. Chang, H. Guan, Y. Gong, Y. Kuang, Y. Yu, D. Dai, and Z. Li, "Dual functional WDM devices for multiplexing and de-multiplexing on silicon-on-insulator," in the international photonics and optoelectronics meeting 2017 (Optical Society of America, 2017), paper AS3A.25.
4. Q. Liu, Z. L. Ran, Y. J. Rao, S. C. Luo, H. Q. Yang, and Y. Huang, "Highly integrated FP/FBG sensor for simultaneous measurement of high temperature and strain," in IEEE Photon. Technol. Lett. **26**, 1715-1717 (2014).
5. B. Ratni, S. N. Burokur, A. de Lustrac, D. Guihard, and B. Rmili, "Directive reconfigurable Fabry-Perot cavity antenna for space applications," in *Proc. 6th IEEE International Conference on Wireless for Space and Extreme Environments-WiSEE* (Huntsville, AL, USA, 2018), pp. 104-106.
6. S. Takashina, Y. Mori, H. Hasegawa, K. Sato, and T. Watanabe, "Wavelength-tunable filters utilizing arrayed waveguide gratings for colorless/directionless/contentionless optical signal drop in ROADMs," IEEE Photon. J. **7**, 1-11 (2015).
7. S. A. Azizan, M. S. Azmi, and Y. Maeda, "Multicasting characteristics of all-optical triode based on negative feedback optical amplifiers," Global J. Res. Eng. **15**, 1-5 (2015).
8. H. Zhang, L. Zhou, J. Xu, L. Lu, J. Chen, and B. M. A. Rahman, "All-optical non-volatile tuning of an AMZI-coupled ring resonator with GST phase-change material," Opt. Lett. **43**, 5539-5542 (2018).
9. J. Li, Q. Huang, R. Yin, W. Ji, Z. Gong, and Z. Song, "Customizable optical pressure sensor based on optimized asymmetric Mach-Zehnder interferometer," IEEE Sensors J. **20**, 8903-8911 (2020).
10. C. Ma, T. Liu, K. Liu, J. Jiang, Z. Ding, L. Pan, and M. Tian, "Long-range distributed fiber vibration sensor using an asymmetric dual Mach-Zehnder interferometers," J. Lightwave Technol. **34**, 2235-2239 (2016).
11. M. Bianchetti, M. S. Avila-Garcia, R. I. Mata-Chavez, J. M. Sierra-Hernandez, L. A. Zendejas-Andrade, D. Jauregui-Vazquez, J. M. Estudillo-Ayala, and R. Rojas-Laguna, "Symmetric and asymmetric core-offset Mach-Zehnder interferometer torsion sensors," IEEE Photon. Technol. Lett. **29**, 1521-1524 (2017).
12. Y. Xiao, M. Hofmann, Z. Wang, S. Sherman, and H. Zappe, "Design of all-polymer asymmetric Mach-Zehnder interferometer sensors," Appl. Opt. **55**, 3566-3573 (2016).
13. B. Wang, Y. Niu, S. Zheng, Y. Yin, and M. Ding, "A high temperature sensor based on sapphire fiber Fabry-Perot interferometer," IEEE Photon. Technol. Lett. **32**, 89-92 (2020).
14. X. Wu, Y. Wang, Q. Chen, Y.-C. Chen, X. Li, L. Tong, and X. Fan, "High-Q, low-mode-volume microsphere-integrated Fabry-Perot cavity for optofluidic lasing applications," Photon. Res. **7**, 50-60 (2019).
15. A. A. Sayem and S. Rahman, "Tunable Fabry Perot filter using all-dielectric multilayer anisotropic metamaterial in the mid-infrared frequency range," in *Proc. 9th International Conference on Electrical and Computer Engineering -ICECE* (Dhaka, Bangladesh, Dec. 2016), pp. 361-364.
16. H. Li, Q. Zhao, S. Jiang, J. Ni, and C. Wang, "FP cavity and FBG cascaded optical fiber temperature and pressure sensor," Chin. Opt. Lett. **17**, 040603- (2019).
17. R. Oliveira, L. Bilro, and R. Nogueira, "Fabry-Pérot cavities based on photopolymerizable resins for sensing applications," Opt. Mater. Express **8**, 2208-2221 (2018).
18. A. Vaz, N. Barroca, M. Ribeiro, A. Pereira, and O. Frazão, "Optical fiber humidity sensor based on polyvinylidene fluoride Fabry-Perot," IEEE Photon. Technol. Lett. **31**, 549-552 (2019).
19. X. Guo, J. Zhou, C. Du, and X. Wang, "Highly sensitive miniature all-silica fiber tip Fabry-Perot pressure sensor," IEEE Photon. Technol. Lett. 31, 689-692 (2019).
20. Q. Deng, L. Liu, X. Li, and Z. Zhou, "Arbitrary-ratio 1×2 power splitter based on asymmetric multimode interference," Opt. Lett. **39**, 5590-5593 (2014).